

Isotopic ratios in the red giant component of the recurrent nova T Coronae Borealis

Ya.V. Pavlenko^{1,2*}, A. Evans³, D. P. K. Banerjee⁴, T. R. Geballe⁵, U. Munari⁶,
R. D. Gehrz⁷, C. E. Woodward⁷, S. Starrfield⁸

¹Main Astronomical Observatory, Academy of Sciences of the Ukraine, Golosiiv Woods, Kyiv-127, 03680 Ukraine

²Centre for Astrophysics Research, University of Hertfordshire, College Lane, Hatfield, AL10 9AB, UK

³Astrophysics Group, Lennard Jones Laboratory, Keele University, Keele, Staffordshire, ST5 5BG, UK

⁴Physical Research Laboratory, Navrangpura, Ahmedabad, Gujarat 380009, India

⁵Gemini Observatory, 670 N. Aohoku Place, Hilo, HI, 96720, USA

⁶INAF Astronomical Observatory of Padova, I-36012 Asiago (VI), Italy

⁷Minnesota Institute for Astrophysics, School of Physics & Astronomy, 116 Church Street SE, University of Minnesota, Minneapolis, MN 55455, USA

⁸School of Earth and Space Exploration, Arizona State University, Box 871404, Tempe, AZ 85287-1404, USA

Version of 28 August 2020

ABSTRACT

We report the determination of abundances and isotopic ratios for C, O and Si in the photosphere of the red giant component of the recurrent nova T Coronae Borealis from new 2.284–2.402 μm and 3.985–4.155 μm spectroscopy. Abundances and isotopic ratios in the photosphere may be affected by (i) processes in the red giant interior which are brought to the surface during dredge-up, (ii) contamination of the red giant, either during the common envelope phase of the binary evolution or by material synthesised in recurrent nova eruptions, or a combination of the two. We find that the abundances of C, O and Si are reasonably consistent with the expected composition of a red giant after first dredge-up, as is the $^{16}\text{O}/^{17}\text{O}$ ratio. The $^{28}\text{Si}/^{29}\text{Si}$ ratio is found to be 8.6 ± 3.0 , and that for $^{28}\text{Si}/^{30}\text{Si}$ is 21.5 ± 3.0 . The $^{12}\text{C}/^{13}\text{C}$ ratio (10 ± 2) is somewhat lower than expected for first dredge-up. The $^{16}\text{O}/^{18}\text{O}$ ratio (41 ± 3) is highly inconsistent with that expected either from red giant evolution (~ 550) or from contamination of the red giant by the products of a nova thermonuclear runaway. In particular the C and O isotopic ratios taken in combination are a puzzle. We urge confirmation of our results using spectroscopy at high resolution. We also encourage a thorough theoretical study of the effects on the secondary star in a recurrent nova system of contamination by ejecta having anomalous abundances and isotopic ratios.

Key words: nuclear reactions, nucleosynthesis, abundances — stars: AGB and post-AGB — stars: abundances — stars: individual (T CrB) — novae: cataclysmic variables — infrared: stars

1 INTRODUCTION

Recurrent novae (RNe) are cataclysmic variable (CV) systems that have been observed to undergo more than one nova outburst (see e.g. Evans et al. 2008, and references therein). They fall into two groups, having short (~ 1 day) and long (~ 1 yr) orbital periods (Anupama 2008), the latter having red giant (RG) secondaries. Long orbital periods demand RG secondaries so that they are sufficiently large either to fill their Roche lobes, or to have large mass-loss rates in the form of winds.

Most RNe are believed to have white dwarf (WD) primaries

with masses close to the Chandrasekhar limit. Like classical novae, RN eruptions are the result of a thermonuclear runaways (TNRs) on the surfaces of the WD components. The recurrence time-scales for both types of RNe range from ~ 10 yrs to ~ 80 yrs (see Schaefer 2010, and references therein), which (in part at least) is an observational selection effect.

The RN T CrB has undergone eruptions in 1866 and 1946, and there are several indicators to suggest that another eruption is imminent (Schaefer 2010; Munari, Dallaporta & Cherini 2016). The system has a long orbital period (227.67 d). The spectral type of the RG is M3 III (Anupama 2008). Three studies have found that the mass of the WD is $\sim 1.35 M_{\odot}$ (Shahbaz et al. 1997; Kennea et al.

* E-mail: yp@mao.kiev.ua

2009; Shara et al. 2018), which is close to the Chandrasekhar limit. Shara et al. give $2.1 \times 10^{-8} M_{\odot} \text{ yr}^{-1}$ for the mass accretion rate.

Evans et al. (2019) recently presented NASA *Spitzer Space Telescope* (Werner et al. 2004; Gehrz et al. 2007), *Stratospheric Observatory for Infrared Astronomy* (SOFIA; Young et al. 2012) and other infrared (IR) observations of T CrB. They reported the discovery of the SiO $8 \mu\text{m}$ fundamental transition in absorption, arising from both the RG photosphere and its wind.

Isotopic abundances of the elements in stars, supernovae and meteors are good indicators of nucleosynthetic processes in the Galaxy. In particular, the isotopes of carbon, oxygen and silicon form under very specific conditions. Knowledge of the isotopic compositions in stars is an important factor in understanding Galactic chemical evolution (see e.g. Romano et al. 2017). Using the first overtone of CO in absorption, Evans et al. (2019) determined that the photospheric $^{12}\text{C}/^{13}\text{C}$ ratio is $\lesssim 9$ in the RG in T CrB; this is considerably lower than the Solar System value of 89 (e.g. Asplund et al. 2009).

The abundances of C, O and Si isotopes in the RG in T CrB may differ from those in “field” RGs, as it might be contaminated by material from the WD progenitor (e.g. during the common envelope phase), or by ejecta from RN eruptions. In the latter case for example, enhancements of ^{17}O and ^{13}C might occur, depending on the nature of the RN eruption, but no significant enhancements of the Si isotopes should occur unless the WD is of the ONe type (see e.g. Starrfield et al. 2009).

Here we present near IR spectra at higher resolution than in Evans et al. (2019), to isolate various isotopic bands. We determine abundances and isotopic ratios for carbon, oxygen and silicon in the RG photosphere. Following Evans et al. (2019), we assume a reddening of $E(B - V) = 0.06$.

2 OBSERVATIONS

Spectra of T CrB were obtained in April 2019 at the Frederick C. Gillett Gemini North Telescope for program GN-2019A-FT-207. The facility near-infrared spectrograph GNIRS was used with its $111 \ell \text{ mm}^{-1}$ grating, long focal length camera, a $0.10''$ diameter slit, and in the normal stare/nod-along-slit mode. An observing log is provided in Table 1. Two slightly overlapping spectral segments, each in the regions of the CO first overtone bands at $2.3\text{--}2.4 \mu\text{m}$ and the SiO overtone bands at $4.0\text{--}4.15 \mu\text{m}$, were observed. A telluric standard star near T CrB (see Table 1) was observed either immediately before or immediately after T CrB to ensure close airmass matches.

Data reduction, utilising IRAF (Tody 1986, 1993) and FIGARO (Shorridge et al. 2014), was mostly standard, consisting of flat-fielding, spectrum extraction, spike removal, combining spectra from the nodded positions, wavelength calibration (using telluric lines; accurate to $0.00003 \mu\text{m}$ for the CO spectra and $0.00006 \mu\text{m}$ for the SiO spectra), ratioing T CrB spectra by the standard spectra, and stitching together the adjacent segments. In the shorter wavelength SiO spectrum the standard star’s spectrum contains prominent H I 5–4 and 14–6 absorption lines. To remove them from its spectrum prior to ratioing the same technique as described in Stencil et al. (2015) was employed.

There is evidence that the RG in T CrB is irradiated by the WD (see Evans et al. 2019) and we note that the orbital phase on the date of the Gemini observation was 0.13, with 0.0 corresponding

to the RG near inferior conjunction (i.e., in front of the WD). We therefore ignore the effects of irradiation of the RG by the WD.

3 SYNTHETIC SPECTRA

Theoretical synthetic spectra were computed using the program WITA6 (see Pavlenko & Jones 2002; Pavlenko, Jones & Longmore 2003; Pavlenko, Yurchenko & Tennyson 2020a; Ivanyuk et al. 2017, for details). We assumed local thermodynamic equilibrium (LTE), hydro-static equilibrium and a one-dimensional (1D) model atmosphere without sources and sinks of energy. Synthetic spectra were computed for RG model atmospheres having effective temperatures $T_{\text{eff}} = 3000 - 4000 \text{ K}$, gravities $\log g$ from 0 to 3 with an increment $\Delta \log g = 1.0$, and microturbulent velocity 3 km s^{-1} . The model atmosphere parameters for the T CrB RG were determined in Evans et al. (2019) and Woodward et al. (2020).

Molecular line lists were taken from the High-temperature Molecular Spectroscopic Database (HITEMP; Rothman et al. 2010). Data for SiO and its isotopologues were taken from the Molecular line lists for Exoplanet and other Hot Atmospheres (ExoMol; Barton et al. 2013) database. The Einstein A coefficients in the ExoMol line list for SiO are accurate to about 10–20% (S. Yurchenko, private communication). The uncertainties in A will of course impact our abundance uncertainties, but for consistency with the CO analysis and with previous work, we do not propagate these uncertainties into our final results. The dissociation energy of SiO was taken to be 8.26 eV (see e.g. Cox 2000). H_2O was accounted for using the “BT2” line list (Barber et al. 2006). Computations, which included all the most abundant isotopologues of CO and SiO, were performed for the 1D SAM12 model atmospheres (Pavlenko et al. 2003).

The best fits to the observed spectra were determined by minimising the function $S = \sum_i^n s_i^2$, where

$$s_i = |(F_i^{\text{obs}} - F_i^{\text{comp}})|, \quad i = 1, n;$$

$F_i^{\text{obs}}, F_i^{\text{comp}}$, n are the observed and computed fluxes at n wavelengths, respectively. The minimisation parameter S is found iteratively on the 3D grid of radial velocity sets, normalisation factors, and broadening parameters. We also compute the errors in the fits $\delta = \sum_i s_i/n$.

To accelerate the iteration process, the theoretical spectrum is normalised to have flux 1.0 at the maximum of the spectral energy distribution (SED); accordingly the fitted and observed spectra are displayed here with flux in the range 0–1. For each spectrum we determine the “effective” resolution R , which differs from the nominal observational spectral resolution because of the effects of macro/macro-turbulent motions in the stellar atmosphere, etc. Synthetic spectra were computed for a model atmosphere with $[T_{\text{eff}}, \log g, [\text{Fe}/\text{H}]] = [3600, 1.0, 0.0]$, convolved with $R = 8\text{k}, 9\text{k}, 10\text{k}, 11\text{k}, 12\text{k}$, and fitted to the observed spectrum¹. We find that the deduced abundances have only a marginal dependence on T_{eff} . The optimal values of the atomic and isotopic abundances for C and Si were finally determined using the procedure described by Pavlenko et al. (2020b).

¹ Throughout we specify a model with the convention $[T_{\text{eff}}, \log g, [\text{Fe}/\text{H}]]$.

Table 1. Observing log..

UT Date YYYY-MM-DD	Airmass	Spectral range (μm)	Resolution ($R = \lambda/\Delta\lambda$)	Integration time (s)	Telluric Standard (airmass)
2019-04-10	1.02	2.284–2.346	19,000	320	HIP 75178 (1.04)
2019-04-16	1.01	2.342–2.402	19,000	240	HIP 75178 (1.01)
2019-04-19	1.20	4.065–4.155	22,000	640	HIP 75178 (1.18)
2019-04-25	1.12	3.985–4.075	22,000	640	HIP 83207 (1.07)

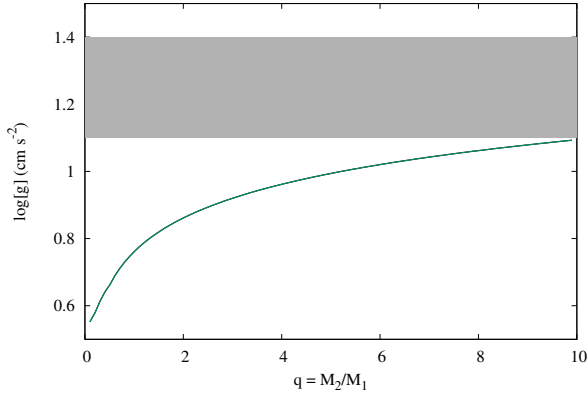


Figure 1. Dependence of $\log g$ on the mass ratio M_2/M_1 . Solid curve corresponds to Equation (1), and applies if the RG fills its Roche lobe. Shaded rectangle is typical $\log g$ for field RGs of spectral type M3III. See text for details.

4 ESTIMATING $\log g$ FOR THE RG

The strengths of the first overtone CO bands in stellar spectra depend on the effective temperature T_{eff} , the elemental and molecular abundances, and gravity $\log g$. We have determined the effective temperature of the RG in T CrB ($T_{\text{eff}} = 3600$ K; Evans et al. 2019) by fitting the 0.75–2.5 μm spectrum (including the TiO bands), on the assumption that the abundances of metals and other molecules are solar.

However, the carbon abundance in the RG in T CrB may differ from solar. Furthermore, $\log g$ is a poorly determined parameter, even for normal RGs. To estimate $\log g$ for the RG in T CrB, we use the reasonably-well constrained values for T CrB, namely the orbital period (227.67 d) and the mass of the WD ($1.35 M_{\odot}$; see Section 1). There is strong evidence, in the form of ellipsoidal variations in the IR (Yudin & Munari 1993), that the RG in T CrB fills its Roche lobe. For our present purposes we assume that it does so, and that the volume of the RG equals the volume of its Roche lobe. The formulae summarised by King (1989) give

$$g = \frac{(GM_1)^{1/3}(4\pi^2)^{2/3}}{P^{4/3}} \frac{q}{(1+q)^{2/3}[f(q)]^2} \approx 1.231 \left(\frac{M_1}{1.35 M_{\odot}} \right)^{1/3} \frac{q}{(1+q)^{2/3}[f(q)]^2} \quad (1)$$

for the surface gravity g (in cm s^{-2}), where $q = M_2/M_1$ is the mass ratio, M_1 (M_2) being the mass of the WD primary (RG secondary) star and $f(q) = R_2/a$ is an empirical function of q that is determined by the ratio of the secondary Roche lobe radius (R_2) and the separation of the stars, a (see King 1989, and especially Section 2.3 therein, for details). The dependence of $\log g$ on

Table 2. Wavelengths (in μm , in vacuo) of the CO band-heads. First overtone transitions are indicated by δv . From <https://www.gemini.edu/observing/resources/near-ir-resources/spectroscopy/co-lines-and-band-heads>.

δv	$^{12}\text{C}^{16}\text{O}$	$^{13}\text{C}^{16}\text{O}$	$^{12}\text{C}^{18}\text{O}$	$^{12}\text{C}^{17}\text{O}$
2–0	2.2935	2.3448	2.3492	2.3226
3–1	2.3227	2.3739	2.3783	2.3517
4–2	2.3525	2.4037	2.4081	2.3815
5–3	2.3829	2.4341	2.4385	2.4119
6–4	2.4142	2.4652	2.4696	—
7–5	2.4461	2.4971	—	—
8–6	2.4787	—	—	—
9–7	2.5122	—	—	—

q from Equation (1) is shown in Fig. 1, in which it is clear that $0.6 \lesssim \log g \lesssim 1.1$ for a wide range of RG/WD mass ratios.

Field M giants generally have masses $\sim 1 - 2 M_{\odot}$ and radii in the range 40–100 R_{\odot} for “normal” early- to mid-M-giants. The corresponding $\log g$ values (in cgs units) are of order 1.0 dex for early-M and middle-M giants (see Gray & Corbally 2009, and references therein); the typical range of $\log g$ for M giants is shown by the shaded region in Fig. 1. For the RG in the T CrB system, $\log g$ is highly unlikely to be greater than this; indeed it is almost certainly smaller as the RG will likely be bloated as a result of irradiation by the WD.

We use $\log g = 1$ and $T_{\text{eff}} = 3600$ K here.

5 ABUNDANCES AND ISOTOPIC RATIOS

5.1 Carbon abundance and the $^{12}\text{C}/^{13}\text{C}$ ratio

The carbon abundance and the C isotopic ratios were determined iteratively by fitting the first overtone CO bands. The band heads for the various CO isotopologues, together with the corresponding individual first overtone transitions, are shown in Fig. 2 and listed in Table 2.

As a rule, lowering $\log g$ increases the strength of CO bands in the synthetic spectra, so that the carbon abundance has to be reduced to fit the observed spectrum. Furthermore, the determined isotopic ratio $^{12}\text{C}/^{13}\text{C}$ is sensitive to changes in the carbon abundance: as $\log N(\text{C})$ is increased, the isotopic ratio $^{12}\text{C}/^{13}\text{C}$ decreases ($N(\text{X})$ being defined as the number of species X). This dependence of $^{12}\text{C}/^{13}\text{C}$ on the C abundance arises because of the different strengths of the ^{12}CO and ^{13}CO features. The ^{12}CO bands are much the stronger, therefore the dependence on changes in the C abundance is much less pronounced. Hence, if we reduce the C abundance, there is a strong reduction in the theoretical ^{13}CO abundance, so we need to increase ^{13}CO by a *larger* amount than the factor by which $N(\text{C})$ was reduced to get the best fit to the observed spectrum. This is illustrated in Fig. 3, which shows the

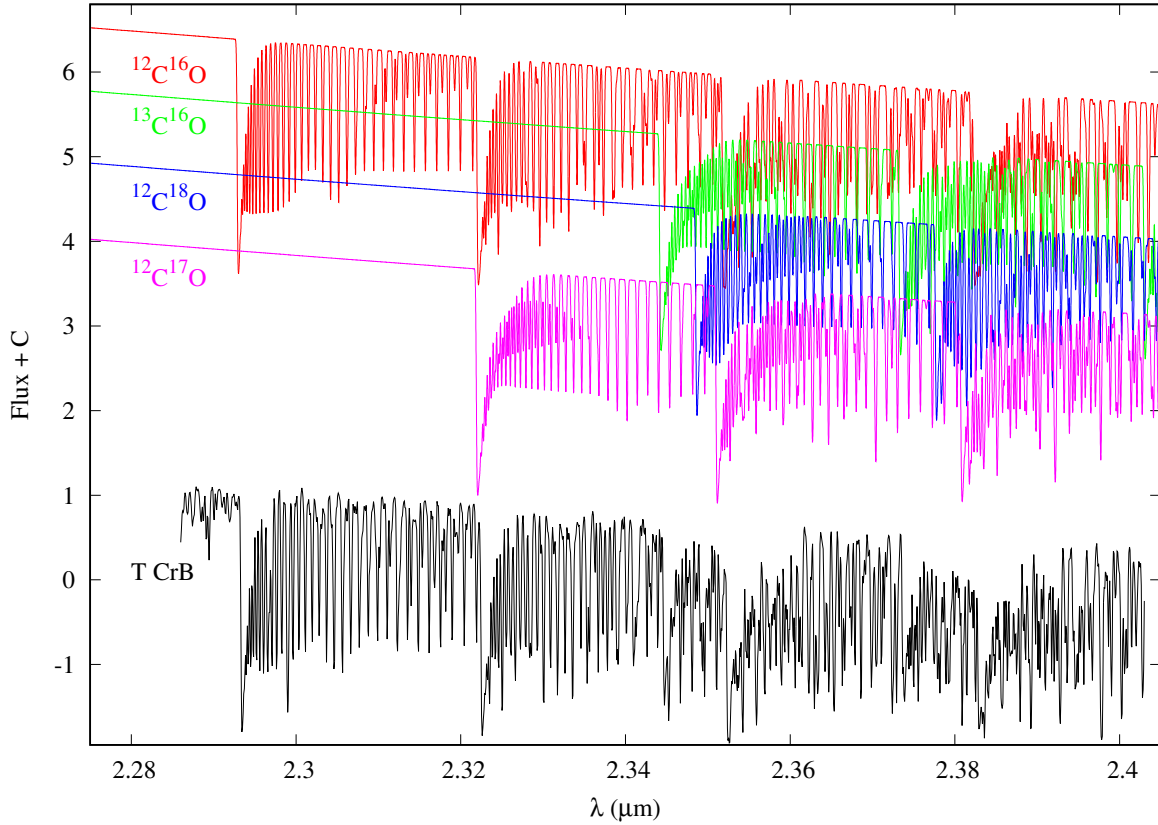


Figure 2. Identification of the isotopic bands of CO. $^{12}\text{C}^{16}\text{O}$: red; $^{13}\text{C}^{16}\text{O}$: green; $^{12}\text{C}^{18}\text{O}$: blue; $^{12}\text{C}^{17}\text{O}$: magenta. The T CrB spectrum is also shown (black). Note that the flux scale is arbitrary.

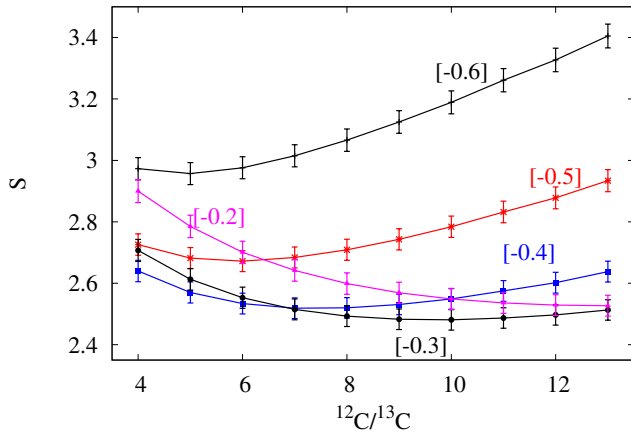


Figure 3. Dependence of minimisation parameter S on the adopted carbon abundance. Numbers in brackets are abundances of carbon measured relative to the solar carbon abundance $\log N(\text{C})_{\odot} = 8.43$ on a scale having $\log N(\text{H}) = 12$ (Asplund et al. 2009).

dependence of the fit parameter S on the assumed carbon abundance. We therefore recomputed the synthetic spectrum for each newly determined carbon abundance.

We also note that the fluxes around the bandheads suffer from some saturation. To overcome this we determine the isotopic ratios and the C abundance using the wavelength range 2.2860–

2.4023 μm , omitting the data around the bandheads (see Fig. 4). We found $^{12}\text{C}/^{13}\text{C} = 10 \pm 2$, $\log N(\text{C}) = 8.09 \pm 0.01$ (on a scale with $\log N(\text{H}) = 12$), i.e. $[\text{C}] = -0.3$, after three iterations². This value of $^{12}\text{C}/^{13}\text{C}$ is consistent with that obtained by Evans et al. (2019; $^{12}\text{C}/^{13}\text{C} \lesssim 9$) using lower resolution spectra.

We show in Fig. 5 the fits to the data with $^{12}\text{C}/^{13}\text{C} = 10$. Also shown are identical models (i.e. same T_{eff} etc.), but with $^{12}\text{C}/^{13}\text{C}$ values that lie outside the deduced uncertainty of ± 2 . This wavelength range covers the $v = 0-2$ transition in $^{13}\text{C}^{16}\text{O}$, and demonstrates that the isotopic ratio deduced provides a good fit to the data, whereas values outside the uncertainty range do not.

5.2 Oxygen isotopic ratios

5.2.1 $^{16}\text{O}/^{18}\text{O}$

For the solar photosphere, $^{12}\text{C}/\text{C} = 0.989$, $^{13}\text{C}/\text{C} = 0.011$; the corresponding data for oxygen are $^{16}\text{O}/\text{O} = 0.99762$, $^{17}\text{O}/\text{O} = 0.000379$, $^{18}\text{O}/\text{O} = 0.0020$ (Asplund et al. 2009).

Our spectra are of sufficient quality that we can determine $^{16}\text{O}/^{18}\text{O}$ for the RG in T CrB. We first model the spectral range 2.28–2.42 μm , which includes all the likely isotopologues of CO. To determine $^{18}\text{O}/^{16}\text{O}$, we fixed $^{12}\text{C}/^{13}\text{C} = 10$ and $\log N(\text{C}) = 7.92$, as found for the [3600/1.0/0.0] model atmosphere (see Section 5.1).

² Including the bandheads results in a value for $^{12}\text{C}/^{13}\text{C}$ of 8.5 ± 0.5

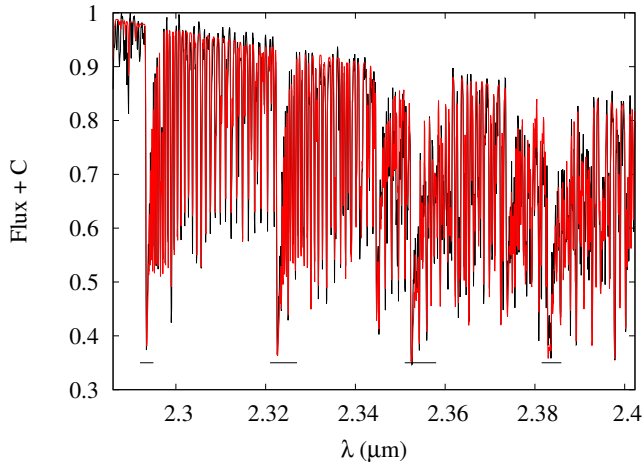


Figure 4. The fit to the first overtone CO bands; the wavelength ranges highlighted by the short lines were omitted from the analysis for reasons discussed in the text.

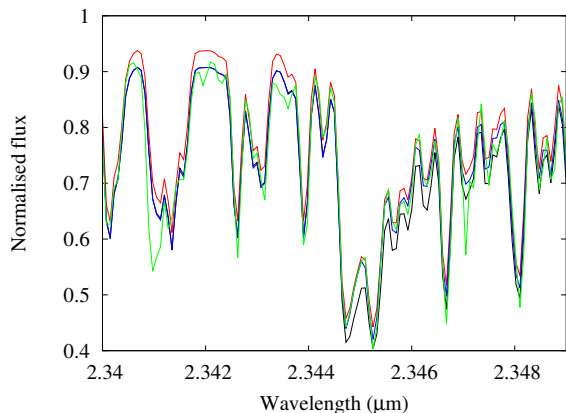


Figure 5. Fit to the CO bands in the 2.340–2.349 μm region. Black curve: T CrB. Green curve: $^{12}\text{C}/^{13}\text{C} = 7$, blue curve: $^{12}\text{C}/^{13}\text{C} = 13$. Red curve: $^{12}\text{C}/^{13}\text{C} = 10$, as discussed in text (see Section 5.1); this curve has been displaced upwards by $+0.03$ to emphasise the difference between it and the green curve, as these are almost indistinguishable shortward of $\sim 2.344 \mu\text{m}$.

The minimisation procedure is run for a set of synthetic spectra with $^{12}\text{C}^{18}\text{O}/\text{CO}$ running from 0 to 0.12, with step size 0.002; in the first iteration we consider the entire spectral range, 2.25–2.4 μm . The dependence of the minimisation parameter S on the $^{12}\text{C}^{18}\text{O}/\text{CO}$ is shown in Fig. 6; there is a weak minimum in S at $^{12}\text{C}^{18}\text{O}/\text{CO} = 0.022$, with an estimated formal error of ± 0.005 .

We then used this result to fine-tune the $^{12}\text{C}^{18}\text{O}$ abundance by confining our analysis to the two specific spectral ranges that contain a significant contribution from $^{12}\text{C}^{18}\text{O}$; these are highlighted in Fig. 6, and shown in detail in Fig. 7, which shows the fit in the region of the 0–2 and 1–3 transitions of $^{12}\text{C}^{18}\text{O}^3$. By fitting the synthetic spectra to this restricted wavelength range, the fit is improved; that this is evident in seen in the top panel of Fig. 6, in

³ Note that, in the case of the model spectrum with no $^{12}\text{C}^{18}\text{O}$, the model drops below the observed spectrum, which does contain $^{12}\text{C}^{18}\text{O}$. This apparent anomaly occurs because, in the minimisation procedure, the absorption by other CO isotopomer(s) has to be increased to attain a better fit.

Table 3. Wavelengths (in μm , in vacuo) of the SiO first overtone bandheads; transitions are indicated by δv . From http://www.ukirt.hawaii.edu/astronomy/calib/spec_cal/sio.html.

δv	$^{28}\text{Si}^{16}\text{O}$	$^{29}\text{Si}^{16}\text{O}$	$^{30}\text{Si}^{16}\text{O}$
2-0	4.004	4.029	4.053
3-1	4.043	4.069	4.092
4-2	4.084	4.109	4.133
5-3	4.125	4.150	4.173
6-4	4.166	—	—

which the synthetic spectrum without $^{12}\text{C}^{18}\text{O}$ (green) provides a significantly poorer fit to the data. We find a better-defined minimum S at

$$^{12}\text{C}^{18}\text{O}/\text{CO} = 0.022 \pm 0.002 .$$

(see Fig. 6, bottom panel, and Fig. 7). We finally find

$$^{16}\text{O}/^{18}\text{O} = N[^{12}\text{C}^{16}\text{O}]/N[^{12}\text{C}^{18}\text{O}] = 41 \pm 3.$$

5.2.2 $^{17}\text{O}/^{16}\text{O}$

The bandheads of $^{12}\text{C}^{17}\text{O}$ nearly overlap with those of $^{12}\text{C}^{16}\text{O}$ (see Fig. 2), which makes problematic the determination of the $^{17}\text{O}/^{16}\text{O}$ ratio. We computed two spectra having relative abundances $N(^{12}\text{C}^{17}\text{O})/N(\text{CO}) = 0.0$ and $= 0.002$, and computed the ratio of the theoretical fluxes. We computed S for three spectral ranges and we conclude that $N(^{12}\text{C}^{17}\text{O})/N(\text{CO}) < 0.002$. This result is consistent with the known low abundance of ^{17}O by comparison with other oxygen isotopes in other environments (e.g. $\sim 4 \times 10^{-4}$ for the solar photosphere; Asplund et al. 2009).

5.3 Silicon isotopic ratios

The presence of the SiO fundamental band near 8 μm in the spectrum of T CrB was reported by Evans et al. (2019). While some of this was photospheric, there was also a contribution from the RG wind, with column density $2.9 \times 10^{17} \text{ cm}^{-2}$. Here we consider the SiO first overtone absorption in the wavelength range 4.00–4.15 μm . The band heads for the various SiO isotopologues, for the various first overtone transitions in the observed wavelength interval, are shown in Fig. 8, and listed in Table 3; absorption by SiO dominates in the above spectral range. As the temperature of the RG wind is $\sim 1000 \text{ K}$ (Evans et al. 2019), we may assume that there is no contribution to the SiO first overtone band heads from the RG wind.

We determined the Si isotopic ratios from the SiO absorption as follows:

(i) As for carbon, we first determined a self-consistent Si abundance and isotopic ratios by varying the abundance of Si in the range $[-0.2, -0.1, 0 +0.1 +0.2]$, and the relative abundance of $^{28}\text{Si}^{16}\text{O}$ in the range 0.90–0.97, with step size 0.01. The process was run iteratively, with model atmosphere and synthetic spectra being recomputed for every new Si abundance until we obtained convergence at $[\text{Si}] = -0.1$.

(ii) We then verified the solution by computing the relative isotopic abundances $N(^{28}\text{Si}^{16}\text{O})/N(\text{SiO})$ and $N(^{29}\text{Si}^{16}\text{O})/N(\text{SiO})$, varied in the ranges $[0.80–0.97]$ and $[0.0–0.2]$, respectively.

The fit to the observed spectrum is shown in Fig. 9. The first

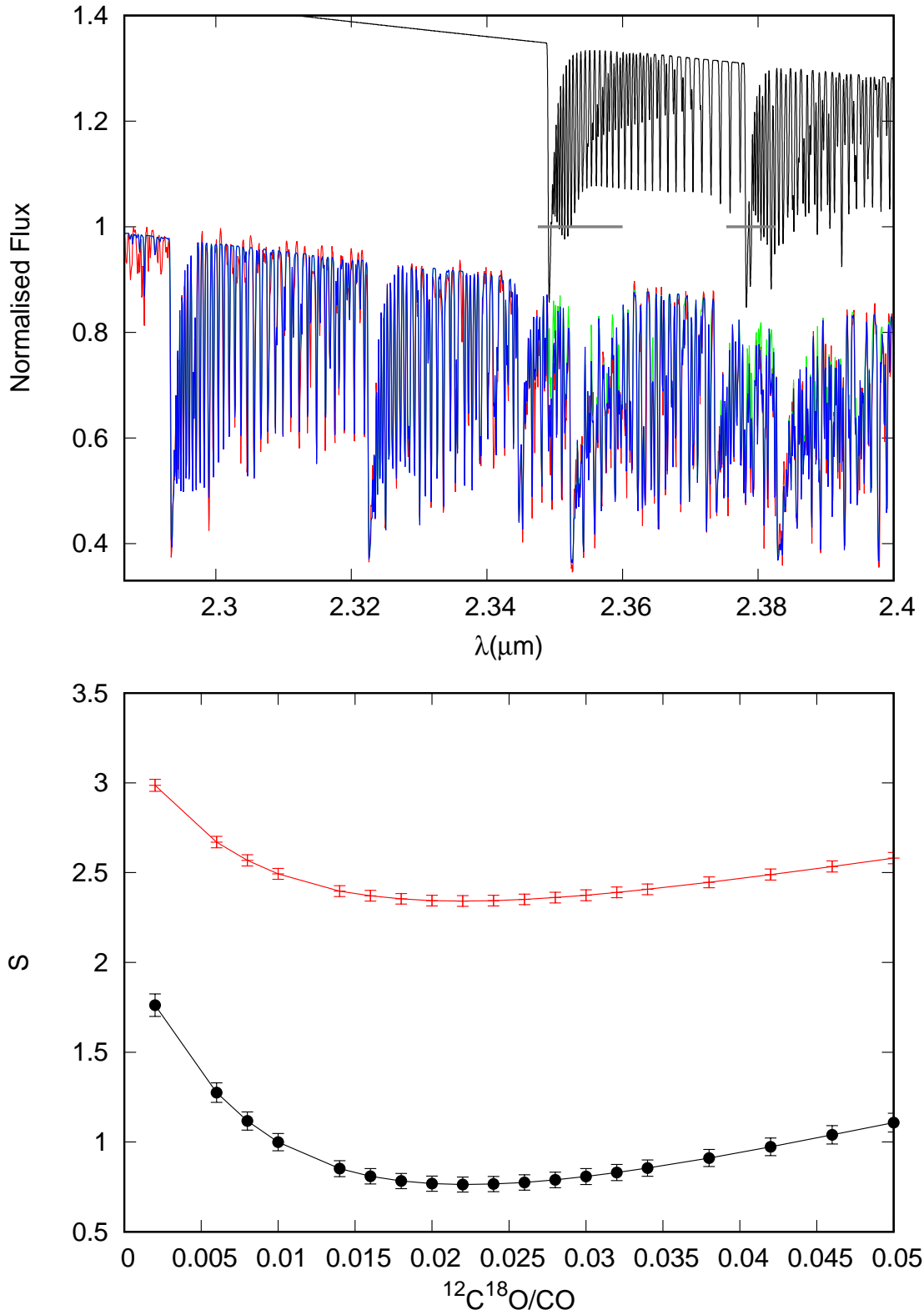


Figure 6. Top: best fit to the observed spectrum (red), with (blue) and without (green) the $^{12}\text{C}^{18}\text{O}$ bands. The $^{12}\text{C}^{18}\text{O}$ bands are shown in black at the top. Bottom: minimisation parameter S for the fit of the synthetic spectra across bands of the first overtone CO over the full spectral region (red line) and across two regions containing the $^{12}\text{C}^{18}\text{O}$ bands (black line), highlighted in the top panel by the horizontal grey lines. See text for details.

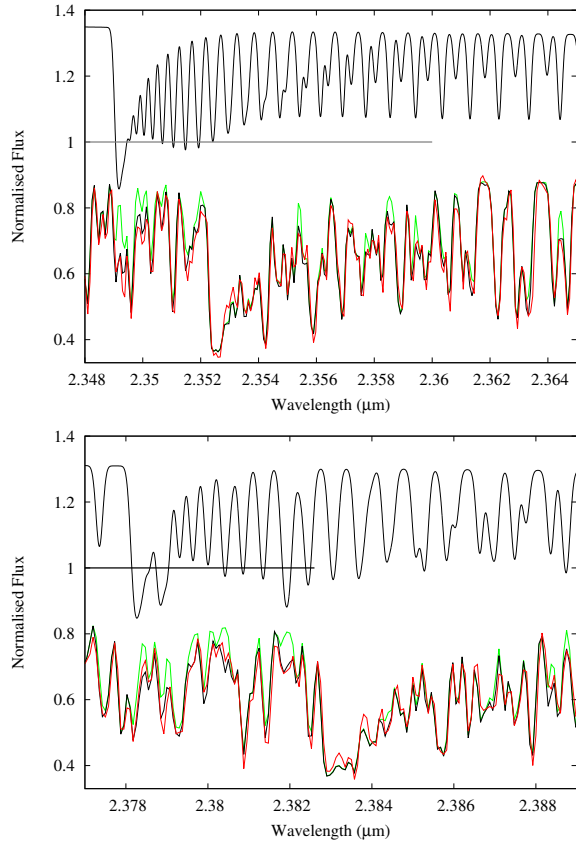


Figure 7. Fits to the two selected spectral regions, defined in the top panel of Fig. 6, containing the 0–2 and 1–3 $^{12}\text{C}^{18}\text{O}$ bandheads. In both panels, black curve is T CrB, green curve is model with no $^{12}\text{C}^{18}\text{O}$, red curve is model with $^{12}\text{C}^{18}\text{O}/\text{CO} = 0.023$. The dark grey curve at the top of each panel is the synthetic $^{12}\text{C}^{18}\text{O}$ spectrum. The horizontal lines at Flux = 1.0 shows the spectral ranges used in the minimisation procedure.

overtone bandheads of ^{29}SiO at $4.029\ \mu\text{m}$, $4.069\ \mu\text{m}$ and $4.109\ \mu\text{m}$ are clearly present, those of ^{30}SiO less obviously so. However we must have the constraint that

$$^{28}\text{Si}/\text{Si} + ^{29}\text{Si}/\text{Si} + ^{30}\text{Si}/\text{Si} = 1,$$

as these are the only isotopes of Si. Minimum $S = 0.332 \pm 0.011$ was found. The Si abundances are listed in Table 4, and the isotopic ratios listed in Table 5. We find $28\text{Si}:29\text{Si}:30\text{Si} = 0.86:0.10:0.04$, i.e. $^{28}\text{Si}/^{29}\text{Si} = 8.6 \pm 3.0$; $^{28}\text{Si}/^{30}\text{Si} = 21.5 \pm 3.0$.

6 EXPECTATION FOR ABUNDANCES AND ISOTOPIC RATIOS

6.1 Elemental abundances

The deduced abundances for C, O and Si for the RG in T CrB are summarised in Table 4, in which the uncertainty in the T CrB abundances are ± 0.1 dex; we see that these elements are somewhat deficient compared to the corresponding solar values. The T CrB abundances are similar to those in two field RGs (see Table 4, in which the uncertainties in the field RG abundances are typically ± 0.03 to ± 0.08 ; Smith et al. 2013). However there may be some evidence for a deficiency in C in the RG in T CrB. This may be evidence for CNO burning, in which the abundance of N increases while that of C decreases.

6.2 Processes in the RG interior

For low-mass ($\sim 1\text{M}_{\odot}$) stars on the RG branch, first dredge-up results in significant changes in the photospheric abundances (see Karakas & Lattanzio 2014, for a comprehensive review). These include a reduction in the C/O ratio (from ~ 0.5 to ~ 0.3), together with changes in isotopic ratios; in particular, $^{12}\text{C}/^{13}\text{C}$ declines from the solar value (~ 90) to ~ 20 , $^{16}\text{O}/^{17}\text{O}$ from ~ 2700 to ~ 300 , and an increase of $^{16}\text{O}/^{18}\text{O}$ from 524 to 740.

The predicted decline of the $^{12}\text{C}/^{13}\text{C}$ ratio to ~ 20 is exceeded in a variety of cases, including RGs in metal-rich clusters (with values as low as < 10), and in RGs in globular clusters. Indeed the two field RGs in Table 4 have low $^{12}\text{C}/^{13}\text{C}$ ratios (15 for β And, 12 for δ Oph; Smith et al. 2013). Table 11 of Hinkle et al. (2016) shows that low values of the $^{12}\text{C}/^{13}\text{C}$ ratio in evolved stars are unusual, but not exceptional (see also Pavlenko et al. 2003, and references therein). Such low values of $^{12}\text{C}/^{13}\text{C}$ might point to additional mixing after the first dredge-up, such that more material processed by CN cycling is mixed into the upper photospheric layers. This would result in a decrease in ^{12}C , ^{16}O and ^{18}O , while ^{13}C and ^{17}O would increase.

6.3 Contamination by RN eruptions

6.3.1 A cautionary preamble

During and immediately after a RN explosion, the products of the TNR reach the RG. The fate of these products however is unclear, and the issue of contamination of the RG by a TNR is a complex one, even if the products remain on the surface rather than sweep past the RG without contaminating it. If the products do pollute the RG surface, only one hemisphere of the RG feels the impact of the ejecta, and whether or not the contaminants remain on the RG surface or are convected into the RG interior is an open question. And even if the pollutants remain on the surface, the time it takes for them to propagate over the entire RG surface, and whether contamination from previous RN eruptions remains on the surface, is also unknown. Furthermore, any TNR products deposited on the RG surface would likely eventually be removed by the RG wind.

Given all these caveats and uncertainties, it is unclear to what extent we can directly compare the surface abundances of the RG in T CrB with the products of a TNR. However we summarise here the likely products of the TNR (Tables 4 and 5), and in our discussion in Section 7 we assume for our present purposes that the TNR products pollute the entire RG surface.

6.3.2 The TNR

Starrfield et al. have undertaken a study of the TNR on the surfaces of ONe (Starrfield et al. 2009) and CO (Starrfield et al. 2020) WDs. As the WD in the T CrB system seems to have mass close to the Chandrasekhar limit (Shahbaz et al. 1997; Kennea et al. 2009; Shara et al. 2018), we confine our discussion of these papers to the products of TNR on the high mass end of WDs.

For TNRs on CO WDs, Starrfield et al. (2020) include mixing of WD and accreted material, the latter assumed to have solar composition; they consider mixes of 25%WD:75%accreted, and 50%WD:50%accreted. The expected C, O, Si abundances, and corresponding isotopic ratios for these cases are included in Tables 4 and 5 for WD masses 1.25M_{\odot} and 1.35M_{\odot} . The Tables include the same information for TNRs on the corresponding ONe WDs (Starrfield et al. 2009).

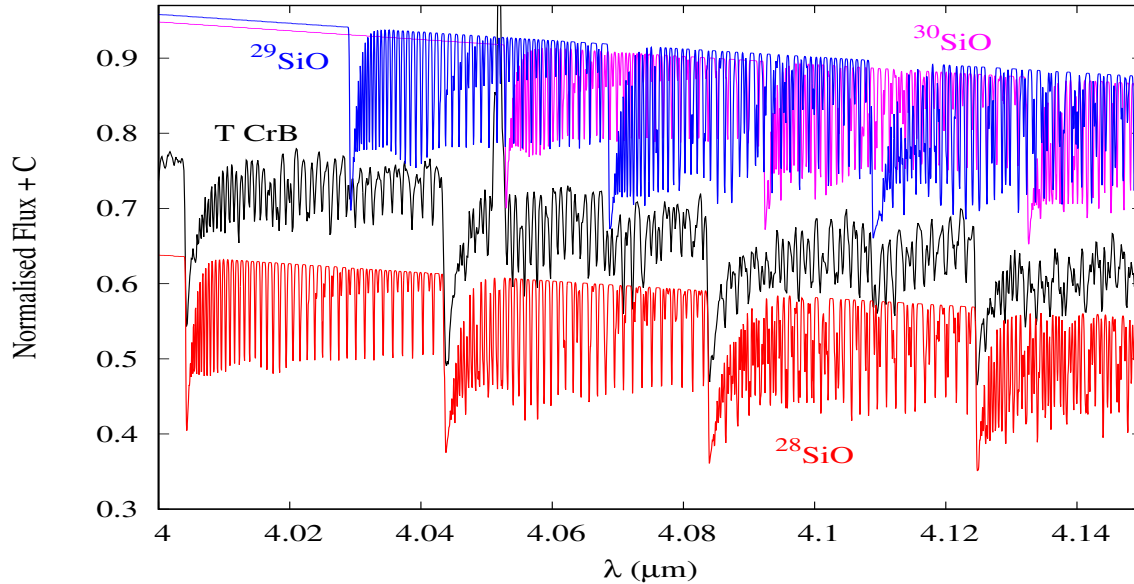


Figure 8. Identification of the SiO isotopologues in the region of the first overtone. T CrB (black curve): ^{28}SiO (red), ^{29}SiO (blue), ^{30}SiO (magenta).

Table 4. Logarithmic abundances (by number) of C, O and Si in the atmosphere of the RG in T CrB and in the solar photosphere, relative to $\log N(\text{H}) = 12$.

Species	T CrB	Solar photosphere ^a	Nova TNR on CO and ONe WDs						Field RGs (β And, δ Oph) ^e
			CO ^b		CO ^c		ONe ^d		
			1.25 M_{\odot}	1.35 M_{\odot}	1.25 M_{\odot}	1.35 M_{\odot}	1.25 M_{\odot}	1.35 M_{\odot}	
C	-3.92	-3.62	-2.10	-1.78	-1.92	-1.76	-2.74	-2.60	-3.81
O	-3.36	-3.36	-2.65	-3.27	-1.52	-1.86	-1.78	-1.83	-3.22
Si	-4.69	-4.54	-3.96	-4.23	-3.41	-3.63	-1.96	-1.52	-4.65

^aAsplund et al. (2009).

^bStarrfield et al. (2020). 25:75 mixing during TNR.

^cStarrfield et al. (2020). 50:50 mixing during TNR.

^dStarrfield et al. (2009); I2005A models.

^eSmith et al. (2013). Value for C includes ^{12}C and ^{13}C ; value for O is for the ^{16}O isotope only.

Starrfield et al. (2009, 2020) find that TNRs on massive WDs of both CO and ONe types produce large overabundances of ^{13}C and ^{17}O , while overabundances of ^{18}O are produced on ONe WDs, and on CO WDs if 75% of the accreted material partakes in the TNR. However only TNRs on ONe WDs synthesise substantial amounts of Si, with both 1.25 M_{\odot} and 1.35 M_{\odot} ONe WD producing overabundances of ^{28}Si , ^{29}Si and ^{30}Si .

7 IMPLICATIONS FOR T CrB

We first note that Si in the photosphere of the RG in T CrB is not overabundant, and is close to that in the solar photosphere and in field RGs (see Table 4). Thus if the RG is polluted by the products of a TNR then the latter is unlikely to have occurred on an ONe WD.

However our deduced $^{12}\text{C}/^{13}\text{C} = 10$ is low, and could be the outcome of either the additional mixing discussed in Section 6.2, or of contamination of the RG photosphere by material from previous RN outbursts. As summarised in Table 5, a TNR can result in a $^{12}\text{C}/^{13}\text{C}$ ratio close to unity (Starrfield et al. 2009, 2020): the ratio in the RG in T CrB does not discriminate between these two scenarios. Similar values of $^{12}\text{C}/^{13}\text{C}$ to that in T CrB have also been found in Miras (e.g. Hinkle, Lebzelter & Straniero 2016).

In a 1 M_{\odot} RG, a ratio of $^{16}\text{O}/^{17}\text{O} \sim 2700$ is predicted after the first dredge-up (Karakas & Lattanzio 2014), and as we are able to place only a lower limit on the $^{16}\text{O}/^{17}\text{O}$ ratio (> 500) in T CrB, we are unable to use this to determine whether the low $^{12}\text{C}/^{13}\text{C}$ ratio is the result of contamination from a RN eruption, or additional mixing following first dredge-up. The ^{17}O abundance in T CrB may be normal for a RG, and is not inconsistent with the values found in Miras (Hinkle et al. 2016) and in some field RGs (see Table 4).

On the other hand, ^{18}O appears to be overabundant in T CrB, as suggested by the deduced ratio of $^{16}\text{O}/^{18}\text{O} \sim 41$. The predicted value is ~ 550 for a 1 M_{\odot} RG, both before and after first dredge-up, while in the solar neighbourhood, its value is ~ 500 (Harris & Lambert 1984; Geiss, Gloeckler & Charbonnel 2002; Scott et al. 2006, and references therein). The anomalous nature of the C and O isotopic ratios for T CrB are highlighted in Fig. 11, in which we have plotted the isotopic ratios for T CrB and the M stars in Hinkle et al. (2016)'s compilation (omitting carbon and S stars). The isotopic ratios for T CrB are clear outliers in the isotopic ratio planes.

Large excesses of ^{18}O have been found in highly evolved objects, for example in several hydrogen-deficient and R CrB stars, with the $^{16}\text{O}/^{18}\text{O}$ ratios being close to, and in some cases less than, unity (Clayton et al. 2007). However, the events that have been pro-

Table 5. Isotopic ratios (by number) for C, O and Si in the atmosphere of the RG in T CrB.

Isotope ratio	T CrB	Solar photosphere ^a	Nova TNR on CO and ONe WDs						RG, with initial mass 1 M _⊙ , after 1st dredge-up ^e
			CO ^b		CO ^c		ONe ^d		
			1.25 M _⊙	1.35 M _⊙	1.25 M _⊙	1.35 M _⊙	1.25 M _⊙	1.35 M _⊙	
¹² C/ ¹³ C	10 ± 2	89	1.3	1.4	1.0	3.9	1.8	2.8	26.3
¹⁶ O/ ¹⁷ O	> 500	2625	0.1	0.17	0.61	0.63	1.3	0.04	2760
¹⁶ O/ ¹⁸ O	41 ± 3	499	46	9.1	1837	3562	52.9	1.8	556
²⁸ Si/ ²⁹ Si	8.6 ± 3.0	19.74	26.9	29.2	23.6	31.1	5.7	0.2	—
²⁸ Si/ ³⁰ Si	21.5 ± 3.0	29.75	1.9	2.2	2.8	2.3	1.8	0.8	—

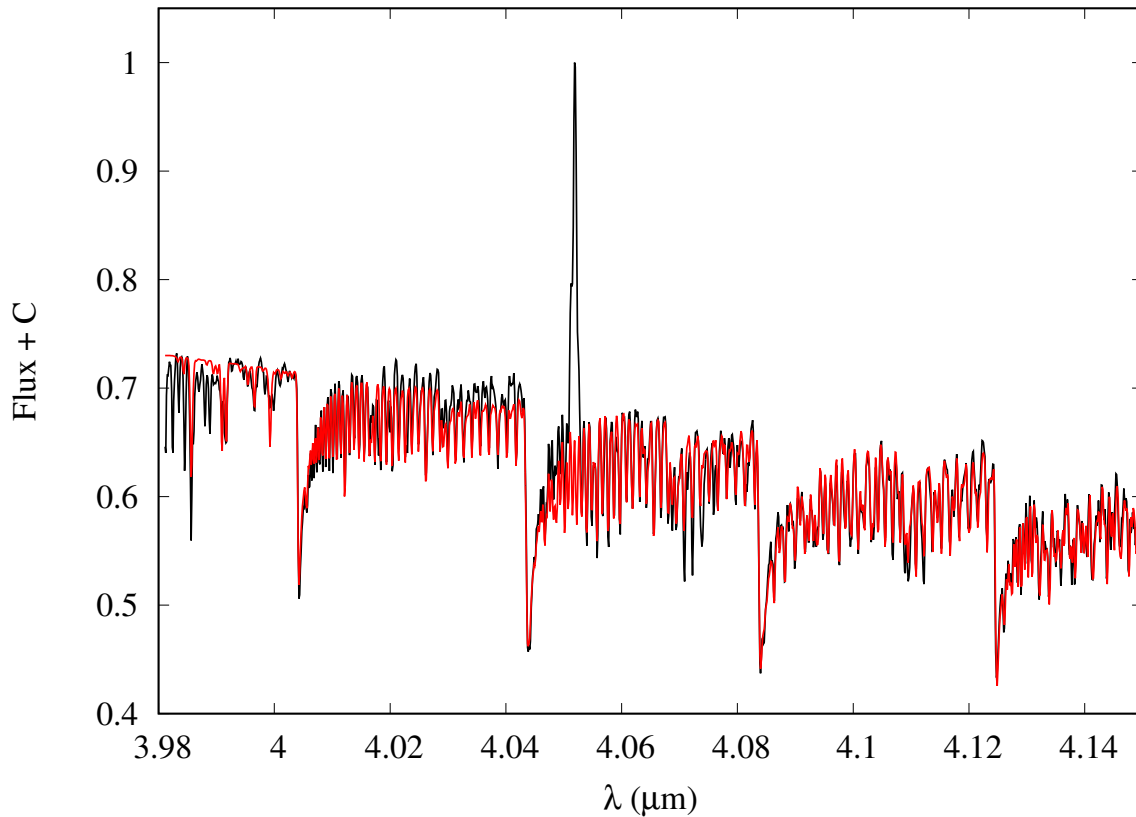
^aAsplund et al. (2009).

^bStarrfield et al. (2020). 25:75 mixing during TNR.

^cStarrfield et al. (2020). 50:50 mixing during TNR.

^dStarrfield et al. (2009); I2005A models.

^eKarakas & Lattanzio (2014).


Figure 9. Fit (red) to the observed spectrum of T CrB (black) across the first overtone SiO bands; the emission feature is Br- α .

posed to produce these unusual values are WD mergers, rather than novae.

We have checked the dependence of the C and Si abundances on effective temperature, and find that a change from 3600 K to 3500 K changes [C] by 0.1, and [Si] by 0.01. Lower values of microturbulent velocity than the 3 km s⁻¹ we have assumed lead to significantly larger values of our fitting parameter S (e.g. $S = 5.77$ for 1 km s⁻¹, and $S = 3.14$ for 2 km s⁻¹, all other parameters being held fixed). We further find that using $\log g = 0$ has negligible effect on S .

We also note that Pavlenko et al. (2020a) recently obtained for the isolated giant Arcturus (K2 III) isotopic ratios $^{12}\text{C}/^{13}\text{C} = 10 \pm 2$ (similar to that found in T CrB) and $^{16}\text{O}/^{18}\text{O} = 2000 \pm 500$

(Pavlenko et al. 2020a). The Arcturus results were obtained using exactly the same procedures as those used here, demonstrating that our results are not a feature of the methodology.

In all these cases the evolutionary histories are of course completely different from that of T CrB. Furthermore, the combined evidence of the $^{16}\text{O}/^{18}\text{O}$ and $^{16}\text{O}/^{17}\text{O}$ ratios in T CrB is extremely puzzling: together they are not compatible with either production in a TNR or in dredge-up.

8 CONCLUSIONS

We have presented near-IR spectroscopy of the RN T CrB and we find that, for the RG in this system:

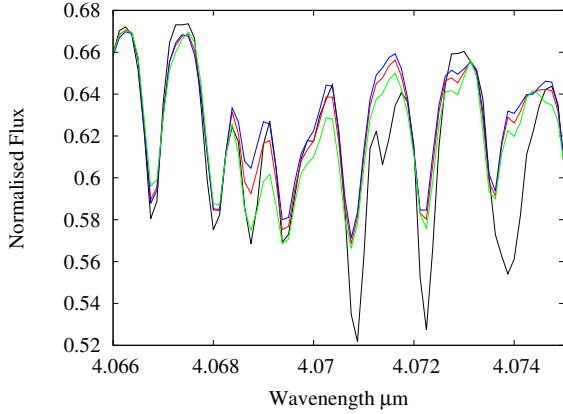


Figure 10. Fit to the SiO bands in the 4.066–4.075 μm region. Black curve: T CrB. Red curve: $^{28}\text{Si}/^{29}\text{Si} = 8.6$, blue curve: $^{28}\text{Si}/^{29}\text{Si} = 6.8$, green curve: $^{28}\text{Si}/^{29}\text{Si} = 13$.

- (i) the $^{16}\text{O}/^{18}\text{O}$ ratio is low, $\sim 41 \pm 3$;
- (ii) the $^{12}\text{C}/^{13}\text{C}$ ratio is 10 ± 2 ;
- (iii) the $^{16}\text{O}/^{17}\text{O}$ ratio is > 500 ;
- (iv) the $^{28}\text{Si}/^{29}\text{Si}$ ratio is 8.6 ± 3.0 ;
- (v) the $^{28}\text{Si}/^{30}\text{Si}$ ratio is 21.5 ± 3.0 .

Taken together, the C and O isotopic ratios are puzzling, and confirmation by obtaining and modelling higher resolution spectroscopy (e.g., $R \sim 60,000$) is highly desirable. Observations of other evolved stars (e.g. field RGs, Miras) at such high resolution have resulted in modelling individually resolved CO lines (Harris & Lambert 1984; Abia et al. 2012; Hinkle, Lebzelter & Straniero 2016)⁴. The results for the $^{16}\text{O}/^{18}\text{O}$ ratio from the latter two studies match very closely for all the stars, with $^{16}\text{O}/^{18}\text{O}$ values between 400 and 500.

We conclude that T CrB shows evidence for a large overabundance of ^{18}O . Whether this is connected with the RG in T CrB being a member of a binary system that periodically undergoes TNR is open to debate. But in addition to the need for verification with high resolution spectroscopy, it is also highly desirable that the extent to which nova ejecta – for both classical and recurrent novae – pollute the atmosphere of the secondary is examined in detail. If the contamination is long-term (i.e. comparable with the inter-outburst period), the implications for the composition of the material accreted on to the WD will be substantial. Understanding this process will be important to understanding the evolution of nova systems.

ACKNOWLEDGMENTS

We thank the referee for their helpful comments on an earlier version of this paper. AE thanks Professor Sergey Yurchenko, UCL, for helpful information about the ExoMol data.

This paper is based on observations obtained for Fast Turnaround programme GN-2019A-FT-207 of the Gemini Observatory, which is operated by the Association of Universities for Research in Astronomy, Inc., under a cooperative agreement with the NSF on behalf of the Gemini partnership: the National

⁴ We note that, while Harris & Lambert (1984) used the CO fundamental band transitions at 4.67 μm , Hinkle et al. (2016) used the CO first overtone transitions.

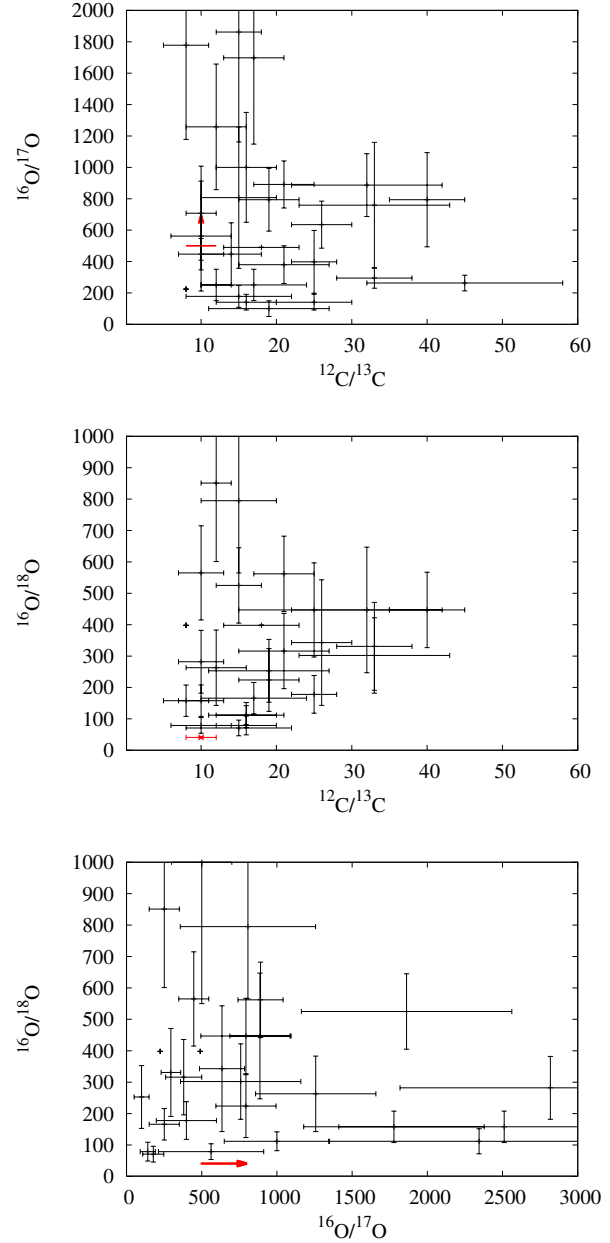


Figure 11. Comparison of the C and O isotopic ratios in T CrB with those in field RGs, as measured by Hinkle et al. (2016). Data for T CrB are in red.

Science Foundation (United States), National Research Council (Canada), CONICYT (Chile), Ministerio de Ciencia, Tecnología e Innovación Productiva (Argentina), Ministério da Ciência, Tecnologia e Inovação (Brazil), and Korea Astronomy and Space Science Institute (Republic of Korea).

YP's work was funded as part of the routine financing program for institutes of the National Academy of Sciences of Ukraine. DPKB is supported by a CSIR Emeritus Scientist grant-in-aid and is being hosted by the Physical Research Laboratory, Ahmedabad. RDG acknowledges support from NASA and the United States Airforce. SS acknowledges partial support to ASU from HST and NASA.

DATA AVAILABILITY

The raw data in this paper are available from the Gemini Observatory Archive, <https://archive.gemini.edu/>

REFERENCES

- Abia C., Palmerini S., Busso M., Cristallo S., 2012, *A&A*, 548, A55
- Anupama G. C., 2008, in *RS Ophiuchi (2006) and the Recurrent Nova Phenomenon*, eds Evans A., Bode M. F., O'Brien T. J., Darnley M. J., *Astronomical Society of the Pacific Conference Series*, vol 401, page 31
- Asplund M., Grevesse N., Sauval A. J., Scott P., 2009, *ARAA*, 47, 481
- Barber R. J., Tennyson J., Harris G. J., Tolchenov R. N., 2006, *MNRAS*, 368, 1087
- Barton E. J., Yurchenko S. N., Tennyson J., 2013, *MNRAS*, 434, 1469
- Clayton G. C., Geballe T. R., Herwig F., Fryer C., Asplund M., 2007, *ApJ*, 662, 1220
- Cox A. N., 2000, *Allen's Astrophysical Quantities*, Fourth edition, ed. A. N. Cox, Springer, New York, Berlin, Heidelberg
- Evans A., Bode M. F., O'Brien T. J., Darnley M. J., 2008, eds *RS Ophiuchi (2006) and the Recurrent Nova Phenomenon*, *Astronomical Society of the Pacific Conference Series* vol 401
- Evans A., et al., 2019, *MNRAS*, 486, 3498
- Gehrz R. D., et al., *Rev. Sci. Inst.*, 78, 011302
- Geiss J., Gloeckler G., Charbonnel C., 2002, *ApJ*, 578, 862
- Gray R. O., Corbally C. J., 2009, *Stellar Spectral Classification* Princeton University Press
- Harris M. J., Lambert D. L., 1984, *ApJ*, 285, 674
- Hinkle K. H., Lebzelter T., Straniero O., 2016, *ApJ*, 825, 38
- Ivanyuk, O. M., Jenkins J. S., Pavlenko Ya. V., Jones H. R. A., Pinfield D. J., 2017, *MNRAS*, 468, 4151
- Karakas A. I., Lattanzio J. C., 2014, *PASA*, 31, e030
- Kennea J. A., Mukai K., Sokoloski J. L., Luna G. M. J., Tueller J., Markwardt C. B., Burrows D. N., 2009, *ApJ*, 701, 1992
- King A. R., 1989, in *Classical Novae*, eds M. F. Bode and A. Evans, first edition, Wiley, Chichester, p. 17
- Munari U., Dallaporta S., Cherini G., 2016, *New Astron.*, 47, 7
- Pavlenko Ya. V., Jones H. R. A., 2002, *A&A*, 396, 967
- Pavlenko Ya. V., Jones H. R. A., Longmore A. J., 2003, *MNRAS*, 345, 311
- Pavlenko Ya V., Yurchenko S. N., Tennyson J., 2020a, *A&A*, 633, 52A
- Pavlenko Ya V., Yurchenko S. N., McKemmish, L. K., Tennyson J., 2020b, *A&A*, in press (arXiv 2008.02092)
- Romano D., Matteucci F., Zhang Z. Y., Papadopoulos P. P., Ivison R. J., 2017, *MNRAS*, 470, 401
- Rothman R. S., et al., 2010, *J. Quant. Spect. Rad. Trans.*, 111, 2139
- Schaefer B. E., 2010, *ApJS*, 187, 275
- Scott P. C., Asplund M., Grevesse N., Sauval A. J., 2006, *A&A*, 456, 6750
- Shahbaz T., Somers M., Yudin B., Naylor T., 1997, *MNRAS*, 288, 1027
- Shahbaz T., Hauschildt P. H., Naylor T., Ringwald F., 1999, *MNRAS*, 306, 675
- Shara M. M., Prialnik D., Hillman Y., Kovetz A., 2018, *ApJ*, 860, 110
- Shorridge K., et al. 2014, *Starlink Figaro: Starlink version of the Figaro data reduction software package*, *Astrophysics Source Code Library*, ascl:1411.022
- Smith V. V., et al. 2013, *ApJ*, 765, 16
- Starrfield S., Iliadis C., Hix W. R., Timmes F. X., Sparks W. M., 2009, *ApJ*, 692, 1532
- Starrfield S., Bose M., Iliadis C., Hix W. R., Woodward C. E., Wagner R. M., 2020, *ApJ*, 895, 70
- Stencel R. E., Blatherwick R. D., Geballe T. R., 2015, *AJ*, 149, 109
- Tody D., 1986, *Proc. SPIE*, 627, 733
- Tody D., 1993, in *Astronomical Data Analysis Software and Systems II*, *ASP Conference Series*, Vol 52, eds. R. J. Hanisch, R. J. V. Brissenden, J. Barnes, San Francisco, California, 173.
- Werner M. W., et al., 2004, *ApJS*, 154, 1
- Woodward C. E., Pavlenko Ya. V., Evans A., Wagner R. M., Ilyin I., Strassmeier K. G., Starrfield S., Munari U., 2020, *AJ*, 159, 231
- Young E. T., et al., 2012, *ApJ*, 749, L17
- Yudin B., Munari U., 1993, *A&A*, 270, 165